ACS Photonics

Article

Cite This: ACS Photonics 2017, 4, 2908-2915

pubs.acs.org/journal/apchd5

Strong Plasmon-Phonon Splitting and Hybridization in 2D Materials Revealed through a Self-Energy Approach

Mikkel Settnes,[†,‡,§] J. R. M. Saavedra,[∥] Kristian S. Thygesen,[§,⊥] Antti-Pekka Jauho,[‡,§] F. Javier García de Abajo,[∥,#] and N. Asger Mortensen*[,§,○,△]

[†]Department of Photonics Engineering, [‡]Department of Micro and Nanotechnology, [§]Center for Nanostructured Graphene, and [⊥]Center for Atomic-Scale Materials Design (CAMD), Department of Physics, Technical University of Denmark, DK-2800 Kongens Lyngby, Denmark

[∥]ICFO-Institut de Ciencies Fotoniques, The Barcelona Institute of Science and Technology, 08860 Castelldefels (Barcelona), Spain

[#]ICREA-Institució Catalana de Recerca i Estudis Avançats, Passeig Lluís Companys, 23, 08010 Barcelona, Spain

[○]Center for Nano Optics and [△]Danish Institute for Advanced Study, University of Southern Denmark, Campusvej 55, DK-5230 Odense M, Denmark

Supporting Information

ABSTRACT: We reveal new aspects of the interaction between plasmons and phonons in 2D materials that go beyond a mere shift and increase in plasmon width due to coupling to either intrinsic vibrational modes of the material or phonons in a supporting substrate. More precisely, we predict strong plasmon splitting due to this coupling, resulting in a characteristic avoided crossing scheme. We base our results on a computationally efficient approach consisting in including many-body interactions through the electron self-energy. We specify this formalism for a description of plasmons based upon a tight-binding electron Hamiltonian combined with the random-phase approximation. This approach is valid provided vertex corrections can be neglected, as is the case in conventional plasmon-supporting metals and Dirac-Fermion systems. We illustrate our method by evaluating plasmonic spectra of doped graphene nanotriangles with varied size, where we predict remarkable peak splittings and other radical modifications in the spectra due to plasmon interactions with intrinsic optical phonons. Our method is equally applicable to other 2D materials and provides a simple approach for investigating coupling of plasmons to phonons, excitons, and other excitations in hybrid thin nanostructures.

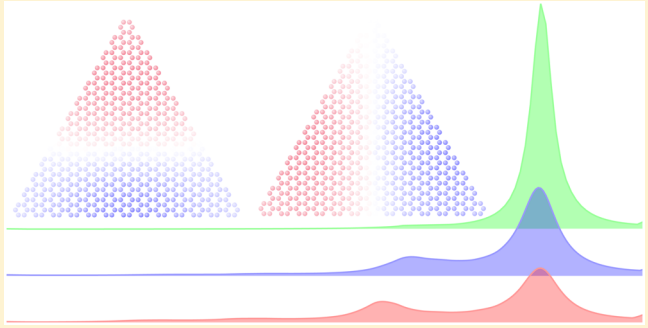

KEYWORDS: *graphene plasmons, quantum plasmonics, nanophotonics, 2D materials, molecular plasmonics, many-body interactions*

Two-dimensional (2D) materials are receiving an increasing interest in nanophotonics due to their ability to host a large variety of polaritons,[1,2] such as tunable plasmon-polaritons in graphene[3,4] or phonon-polaritons in hexagonal boron nitride (h-BN).[5−7] In this context, plasmonics benefits from the unique charge-transport properties of graphene,[8−11] because the electron mobility in a suspended single-atomic-layer can reach 200000 $cm^2\ V^{-1}\ s^{-1}$.[12] Indeed, effects associated with phonon scattering in polarizable substrates[13,14] have been found to be one of the factors limiting the carrier mobility in graphene.[15] Hexagonal boron nitride phonons couple weakly to graphene electrons and this material is therefore suitable for graphene encapsulation compatible with preservation of high mobility.[16−18] When the characteristic energy of plasmons coincides with that of phonons, we anticipate that plasmon−phonon hybridization can take place.[19,20] Actually, strong phonon−plasmon coupled modes have been observed in graphene/SiC[21,22] and graphene/SiO_2 interfaces.[23−25] Likewise, coupling between plasmons and surface phonons has been examined in thin polar substrates.[26−28] Additionally, carrier mobility depends on the electrostatic environment, and has been studied in the context of electrostatic gating of graphene.[29] The influence of substrate-hosted phonons is commonly included through the substrate dielectric function,[8] which qualitatively explains experimental observations rather well.[24,25] Unfortunately, only limited progress has been reported in the quantum description of plasmon-phonon coupling, essentially restricted to analyses based on tight-binding (TB) models combined with the random-phase approximation (RPA).[30−33] More generally, quantum-plasmonic phenomena[34−36] are commonly treated at the single-particle level using various mean-field models,[37−39] often without more explicit accounts for many-body interactions. In this manuscript, we develop an RPA-inspired formalism for the quantum plasmonic response in which the interactions are

Received: August 17, 2017
Published: October 4, 2017

DOI: 10.1021/acsphotonics.7b00928
ACS Photonics 2017, 4, 2908−2915

encoded in the single-electron Green functions through electron−phonon self-energies. As an illustration of our theory, we evaluate the influence of phonons on plasmon resonances in graphene nanotriangles.

Our method is amenable to application in arbitrary graphene geometries and can be directly extended to other plasmon-supporting 2D materials such as black phosphorus[40] and thin noble metals.[41]

THEORETICAL FORMALISM

Within the RPA, the dielectric matrix, $\epsilon(\boldsymbol{r},\boldsymbol{r}',\omega)$, can be expressed in terms of the noninteracting polarizability $\chi^0(\boldsymbol{r},\boldsymbol{r}',\omega)$ as (see, e.g., ref 42)

$$\epsilon(\boldsymbol{r}, \boldsymbol{r}', \omega) = 1 - \sum_{\boldsymbol{R}} V(\boldsymbol{r} - \boldsymbol{R})\chi^0(\boldsymbol{R}, \boldsymbol{r}', \omega) \tag{1}$$

Here, $V(\boldsymbol{r} - \boldsymbol{r}') \propto e^2/|\boldsymbol{r} - \boldsymbol{r}'|$ is the bare Coulomb interaction and the summation is over the atom positions $\boldsymbol{R}$. The formal on-site divergence ($\boldsymbol{r} \to \boldsymbol{r}'$) is only an apparent issue because of the orbitals' finite extension, which is incorporated through a self-interaction term of 0.58 atomic units for $\boldsymbol{r} = \boldsymbol{r}'$.[30,32] The noninteracting polarizability is (see, e.g., ref 42)

$$\chi^0(\boldsymbol{r}, \boldsymbol{r}', \omega) = 2\sum_{nm} [f(\mathcal{E}_m) - f(\mathcal{E}_n)] \times \frac{\psi_n(\boldsymbol{r})\psi_n^*(\boldsymbol{r}')\psi_m^*(\boldsymbol{r})\psi_m(\boldsymbol{r}')}{\hbar\omega + i\eta - \mathcal{E}_n + \mathcal{E}_m} \tag{2}$$

where $f(\mathcal{E})$ is the Fermi−Dirac distribution function and $\mathcal{E}_n$ is the energy associated with the single-electron wave function ψ_n, while η is an infinitesimal broadening. The leading factor of 2 originates in spin degeneracy.

In our account for self-sustained charge-density oscillations (plasmons) that obey Poisson's equation, we here follow the approach of ref 43, that we have previously applied to treat plasmons in monolayer and bilayer transition metal dichalcogenides,[44] graphene,[32] and metallic thin-films[43] and nanowires.[45] Plasmons can exist where the dielectric matrix has zero determinant and the related potential, ϕ, satisfies[43]

$$\sum_{\boldsymbol{R}} \epsilon(\boldsymbol{r}, \boldsymbol{R}, \omega)\phi(\boldsymbol{R}, \omega) = 0 \tag{3}$$

The dielectric matrix may have a finite imaginary part, so eq 3 cannot be satisfied in general for real ω. Instead, we require that the real part vanishes, which defines the plasmon modes ω_n, and the associated potential ϕ_n via[43]

$$\sum_{\boldsymbol{R}} \epsilon(\boldsymbol{r}, \boldsymbol{R}, \omega_n)\phi_n(\boldsymbol{R}, \omega_n) = i\epsilon_n\phi_n(\boldsymbol{r}, \omega_n) \tag{4}$$

Here, ϵ_n is the imaginary part of the eigenvalue of the dielectric matrix $\epsilon(\omega_n)$. Therefore, the plasmon modes are the eigenvectors corresponding to purely imaginary eigenvalues of the dielectric matrix.[43]

Plasmonic spectra can be conveniently analyzed in terms of the electron energy−loss function $-\mathrm{Im}\{\epsilon^{-1}(\omega)\}$, which is relevant for the probing of plasmons in electron energy-loss spectroscopy.[46] Considering the eigenvalues ϵ_n, we effectively calculate the plasmon frequency, ω_n, as the local maximum of $-\mathrm{Im}\{\epsilon^{-1}(\omega)\}$. For a system composed of N atomic sites there exist N eigenvalues and corresponding eigenfrequencies. Below, the main focus is placed on the two eigenvalues with the largest value of $-\mathrm{Im}\{\epsilon^{-1}(\omega_n)\}$, corresponding to doubly degenerate dipolar plasmon resonances.[32] In brief, we can calculate the eigenvalue loss-spectrum and corresponding plasmon modes using the eigenvalues and eigenvectors of the dielectric matrix eq 1. Evidently, this requires an efficient way of calculating $\chi^0(\omega)$. As we now show below, interactions with phonons can readily be included in this scheme.

It is convenient to express the polarizability in terms of the retarded Green function $G_0^r(\boldsymbol{r}, \boldsymbol{r}', \mathcal{E})$ and the spectral function $A_0(\boldsymbol{r}, \boldsymbol{r}', \mathcal{E})$:

$$G_0^r(\boldsymbol{r}, \boldsymbol{r}', \mathcal{E}) = \sum_n \frac{\psi_n(\boldsymbol{r})\psi_n^*(\boldsymbol{r}')}{\mathcal{E} - \mathcal{E}_n + i\eta} \tag{5}$$

$$\begin{aligned} A_0(\boldsymbol{r}, \boldsymbol{r}', \mathcal{E}) &= i[G_0^r(\boldsymbol{r}, \boldsymbol{r}', \mathcal{E}) - G_0^a(\boldsymbol{r}, \boldsymbol{r}', \mathcal{E})] \\ &= 2\pi\sum_n \psi_n(\boldsymbol{r})\psi_n^*(\boldsymbol{r}')\delta(\mathcal{E} - \mathcal{E}_n), \end{aligned} \tag{6}$$

where we also use the advanced Green function, which under the assumption of time-reversal symmetry satisfies $G_0^a(\boldsymbol{r}, \boldsymbol{r}', \mathcal{E}) = [G_0^r(\boldsymbol{r}', \boldsymbol{r}, \mathcal{E})]^*$. Using eqs 5 and 6 while exploiting the symmetry $A(\boldsymbol{r}, \boldsymbol{r}', \mathcal{E}) = A(\boldsymbol{r}', \boldsymbol{r}, \mathcal{E})$, we can express eq 2 in a more general form without any reference to single-particle wave functions,

$$\chi^0(\boldsymbol{r}, \boldsymbol{r}', \omega) = \frac{1}{\pi}\int \mathrm{d}\mathcal{E} f(\mathcal{E})A_0(\boldsymbol{r}, \boldsymbol{r}', \mathcal{E}) \times [G_0^r(\boldsymbol{r}, \boldsymbol{r}', \mathcal{E} + \hbar\omega) + G_0^a(\boldsymbol{r}', \boldsymbol{r}, \mathcal{E} - \hbar\omega)] \tag{7}$$

We focus on the imaginary part of $\chi^0(\omega) = \chi_R^0(\omega) + i\chi_I^0(\omega)$. In the low temperature limit, we thus have[47]

$$\chi_I^0(\boldsymbol{r}, \boldsymbol{r}', \omega) = -\frac{1}{2\pi}\int_{\mathcal{E}_F - \hbar\omega}^{\mathcal{E}_F} \mathrm{d}\mathcal{E}\, A_0(\boldsymbol{r}, \boldsymbol{r}', \mathcal{E})A_0(\boldsymbol{r}, \boldsymbol{r}', \mathcal{E} + \hbar\omega) \tag{8}$$

where $\mathcal{E}_F$ is the Fermi energy. We note that eq 8 can be conveniently written in a convolution form, which allows us to carry out an efficient numerical implementation. The real part of $\chi^0(\omega)$ can then be calculated using the Kramers−Kronig relations with an 8 eV cutoff, as shown in the Supporting Information (SI).

For any system with time-reversal symmetry, the spectral function corresponds to the imaginary part of the Green function $A(\boldsymbol{r}, \boldsymbol{r}', \mathcal{E}) = -2\mathrm{Im}\{G(\boldsymbol{r}, \boldsymbol{r}', \mathcal{E})\}$. Consequently, eq 8 only requires the Green function of the system. This implies an interesting possibility to estimate the effect of interactions: the noninteracting spectral functions in eq 8 can be replaced by interacting Green functions with self-energy insertions. Notably, an energy-dependent, but spatially uniform, self-energy term does not essentially increase the computational burden. The Green function, including an energy-dependent retarded self-energy term $\Sigma(\mathcal{E})$ can be symbolically written as (we suppress the spatial dependence here)

$$\boldsymbol{G}^r(\mathcal{E}) = [\mathcal{E} + i\eta - \boldsymbol{H} - \Sigma(\mathcal{E})]^{-1} \tag{9}$$

The term $\Sigma(\mathcal{E})$ accounts for the interactions between electrons with other degrees of freedom in 2D materials,[48] such as phonons, but it can also account for the lifetime broadening of electron states in open quantum systems where electrons can leak into semi-infinite surroundings.[49] Note that eq 9 contains self-energy corrections to the one-point Green function, while a

DOI: 10.1021/acsphotonics.7b00928
ACS Photonics 2017, 4, 2908−2915

full discussion would require the analysis of a two-point function (i.e., the interacting polarizability). Thus, using eq 9 (and the spectral functions associated with it) implies the omission of vertex corrections. For metals this is a common approach justified by Migdal's theorem,[42] while similar considerations can be made for Dirac materials,[50] given that the sound velocity is much smaller than the Fermi velocity ($v_F \sim 10^6$ m/s for graphene). A quantitative assessment of the role of vertex corrections is however beyond the phenomenological approach adopted in this work.

Recursive Green Function. Many different approaches can be used to determine the Green function $G(\boldsymbol{r}, \boldsymbol{r}', \mathcal{E})$, including brute force inversion or analytical methods. Below, we focus on recursive techniques, which allow us to efficiently deal with large, spatially inhomogeneous systems described by a generic TB Hamiltonian.

We employ the recently developed efficient recursive Green function approach to obtain $\boldsymbol{G}_0^r(\boldsymbol{r}, \boldsymbol{r}', \mathcal{E})$.[51,52] Dividing the system into N_{cell} cells (i.e., with an average of $M = N/N_{cell}$ atoms each) only connecting to neighboring cells, the forward recursion is given by

$$\boldsymbol{g}_1 = (\mathcal{E} + i\eta - \boldsymbol{H}_1)^{-1} \tag{10a}$$

$$\boldsymbol{g}_n = (\mathcal{E} + i\eta - \boldsymbol{H}_n - \Sigma_n)^{-1} \tag{10b}$$

$$\Sigma_n = \boldsymbol{V}_{n,n-1}\boldsymbol{g}_{n-1}\boldsymbol{V}_{n-1,n} \tag{10c}$$

where $\boldsymbol{V}_{n,n-1}$ is the coupling matrix between cell n and cell $n-1$. The last cell contains the full Green function $\boldsymbol{G}$ of that cell. To obtain the entire Green function matrix, we save $\boldsymbol{g}_n$ from the forward recursion and do a backward recursive sweep consisting in updating all diagonal and off-diagonal blocks according to

$$\boldsymbol{G}_n = \boldsymbol{g}_n + \boldsymbol{g}_n\boldsymbol{V}_{n,n-1}\boldsymbol{G}_{n-1}\boldsymbol{V}_{n-1,n}\boldsymbol{g}_n \tag{11a}$$

$$\boldsymbol{G}_{n,m} = \boldsymbol{g}_n\boldsymbol{V}_{n,n-1}\boldsymbol{G}_{n-1,m} \tag{11b}$$

This yields the total Green function for a given energy. For more details on the approach, see SI.

Using this recursive scheme, the computational scaling changes from $O(N_\omega N^3)$ to $O(N_\omega N_{cell} M^3)$, where N_ω is the number of energy points required to perform the integration in eq 8.

The convolution yielding $\chi_I^0(\omega)$ can be done using fast Fourier transforms, yielding a scaling of $O(N \log N)$. A similar scaling is obtained for the Kramers–Kronig transformation, giving a total scaling of the method $O(N_\omega N_{cell} M^3)$.

PLASMONS IN GRAPHENE NANOTRIANGLES

We describe the electronic structure of graphene using a nearest-neighbor TB model $H = -t_0 \sum_{\langle i,j \rangle} c_i^\dagger c_j$, where $t_0 = 2.8$ eV, while the sum runs over all neighbor pairs $\langle i, j \rangle$. To account for a finite carrier density, we choose a Fermi energy $\mathcal{E}_F = 0.4$ eV, which is a typical value in experiments exploring plasmon-phonon coupling.[25] As an illustrative example, we consider graphene nanotriangles with armchair edges because these have a smooth evolution of the electronic states when increasing size.[53,54] Graphene nanostructures such as nanodisks do not necessarily conserve their edge-configuration of atoms when their size is varied (i.e., the emergence of localized edge states may drastically change both the electronic structure and the plasmon response when changing size[30,31]). In the following, we focus on the armchair edge configuration to suppress the complexity added by the appearance of edge states formed at zigzag edges.[31,55] We anticipate that extensions to lattice terminations supporting electronic edge states could bring interesting new physics where the interplay with plasmon–phonon coupling can be explored with the present formalism.

First, we calculate the eigenvalue loss-spectrum for an armchair nanotriangle with side length ~8.1 nm (see Figure 1).

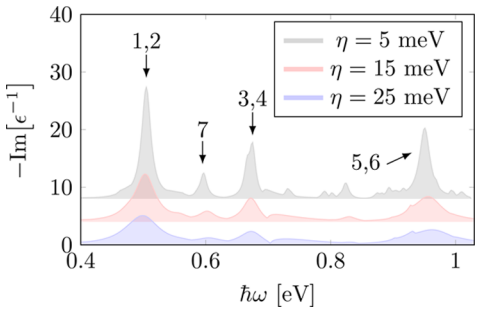

Figure 1. Eigenvalue loss spectrum for an armchair nanotriangle with side length of 8 nm and different values of the broadening η. The different modes are labeled according to Figure 2.

Multiple plasmon peaks are clearly identifiable in the spectrum, with all plasmonic resonances appearing above 0.4 eV for the given choice of Fermi energy and structure dimensions. Inspection of the individual eigenvalues reveals that each peak is either nondegenerate or consists of a pair of eigenstates with double degeneracy. This is consistent with group theory considerations.[32,56] Figure 2 shows the real part of the scalar potential eigenstate ϕ_n for the plasmon peaks labeled in Figure 1. Clearly, $\mathrm{Re}\{\phi_n\}$ reveals a double degeneracy for the modes 1–6, whereas the plasmon mode labeled 7 is nondegenerate. The doubly degenerate modes 1–6 are either symmetric or antisymmetric with respect to the mirror plane. We expect the strongest coupling from an external optical source to the dipole modes 1–2 with electrical fields polarized along the spatial profile of the mode.

Plasmon–Phonon Coupling. Interaction with phonon modes leads to broadening of the plasmonic peaks because of the associated damping, that is captured by $\mathrm{Im}\{\Sigma\} \neq 0$. A simple, phenomenological way to study the effects due to damping is to vary the η parameter in eq 2. This has been done in Figure 1, where the eigenvalue loss-spectrum is shown for different values of the broadening η. It is clear that the peaks broaden and can develop fine structure, as discussed in ref 30. However, by construction, $\mathrm{Re}\{\Sigma\} = 0$ in this model and there are no changes in the central positions of the spectral components.

Generally, interaction effects are energy-dependent and consequently cannot be captured accurately by a constant broadening. The effect of energy-dependent interactions can be described using a self-energy formalism.[48] As explained above, within the present approach the different interaction effects do not increase the size of the Hilbert space, thus, resulting in just a minor increase in computational demand.

In the calculations presented below, we consider a simple model for the electron–phonon interaction appropriate to describe optical phonons in graphene. We follow the approach of refs 57–59 and consider a dispersionless optical phonon of energy $\hbar\Omega_0 = 0.2$ eV. The treatment, however, is general and can be equally applied to both intrinsic and substrate phonons.

DOI: 10.1021/acsphotonics.7b00928
ACS Photonics 2017, 4, 2908–2915

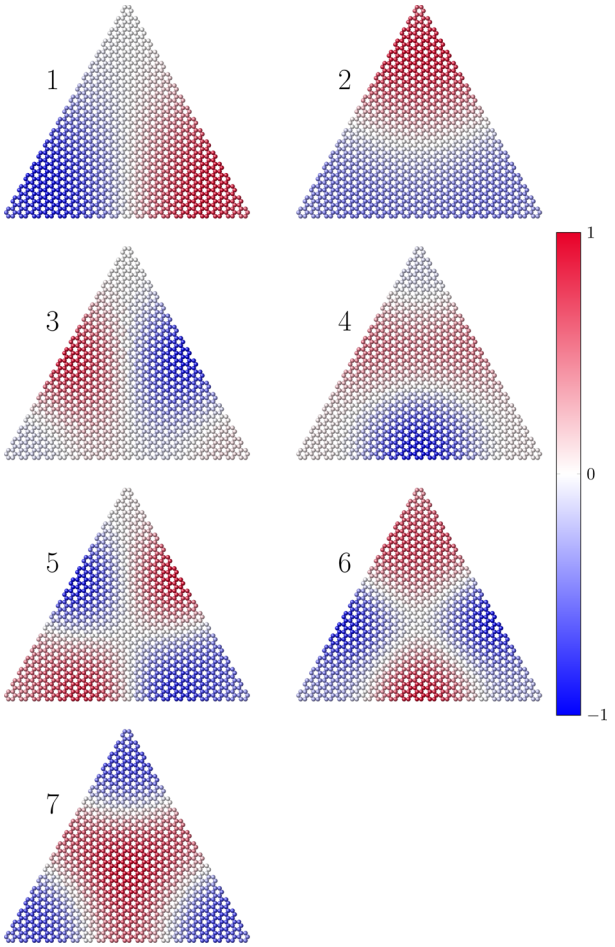

Figure 2. Real space plot of the plasmon scalar potential $\mathrm{Re}\{\phi_n\}$ for the different plasmon modes identified in Figure 1.

For simplicity, we assume a constant electron−phonon matrix element g_0 yielding the on-site self-energy in the Born approximation,[48,57,58]

$$\mathrm{Im}\{\Sigma_{\mathrm{ph}}(\mathcal{E}, T)\} = -\pi|g_0|^2 \int \mathrm{d}\mathcal{E}'\rho_{\mathrm{e}}(\mathcal{E}') \int \mathrm{d}\Omega\rho_{\mathrm{ph}}(\Omega) \times [(n_{\mathrm{B}}(\Omega) + 1 - f(\mathcal{E}'))\delta(\mathcal{E} - \mathcal{E}' - \hbar\Omega) + (n_{\mathrm{B}}(\Omega) + f(\mathcal{E}'))\delta(\mathcal{E} - \mathcal{E}' + \hbar\Omega)] \quad (12)$$

where $|g_0|^2$ is the coupling strength, T is the temperature, $n_{\mathrm{B}}(\Omega)$ is the Bose-Einstein distribution, and $\rho_{\mathrm{ph}}(\Omega)$ is the phonon density of states, which we take to be a Lorentzian centered around $\hbar\Omega_0$ with a phenomenological broadening Δ. Finally, $\rho_{\mathrm{e}}(\mathcal{E})$ is the electron density of states, which can be determined through the recursive algorithm described above as

$$\rho_{\mathrm{e}}(\mathcal{E}) = -(1/\pi) \sum_{\boldsymbol{r}} \mathrm{Im}\{G^r(\boldsymbol{r}, \boldsymbol{r}, \mathcal{E})\}$$

In the low-temperature limit, there is no phonon annihilation, and the expression reduces to

$$\mathrm{Im}\{\Sigma_{\mathrm{ph}}(\mathcal{E}, T \to 0)\} = -\pi|g_0|^2 \int d\Omega\rho_{\mathrm{ph}}(\Omega) \times [(1 - f(\mathcal{E} - \hbar\Omega))\rho_{\mathrm{e}}(\mathcal{E} - \hbar\Omega) + f(\mathcal{E} + \hbar\Omega)\rho_{\mathrm{e}}(\mathcal{E} + \hbar\Omega)] \quad (13)$$

The real part of the self-energy corresponds to the energy shift induced by the interactions and can be conveniently determined using the Kramers−Kronig relation (see details in the SI).

In Figure 3, we show the eigenvalue loss-spectra of nanotriangles of different side lengths with and without

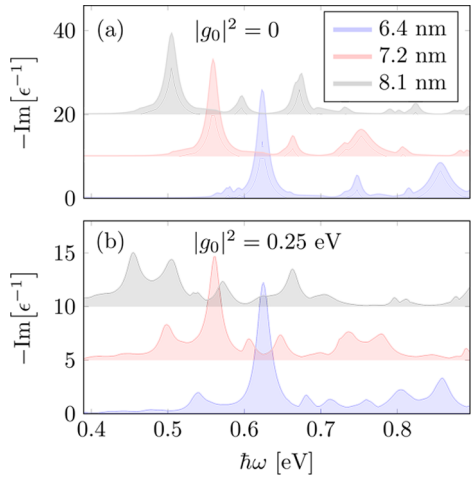

Figure 3. Eigenvalue loss-spectrum for different sizes of armchair graphene nanotriangles, with and without coupling to phonons. Panel (a) uses an energy-independent broadening η = 5 meV, whereas panel (b) includes the phonon interaction with an electron−phonon coupling constant $|g_0|^2$ = 0.25 eV[57,59] and the optical phonon centered at $\hbar\Omega_0$ = 0.2 eV with broadening Δ = 5 meV.

inclusion of the phonon interaction, as described by eq 13. To increase visibility, we have neglected the redshift caused by the real part of the self-energy and aligned the position of the high energy dipole peak to the one without the phonon coupling.

When examining Figure 3a,b, we find a well-known blueshift for decreasing structure size.[24,31] Comparing the two panels, we observe that phonon interaction induces additional peaks in the spectrum, which are caused by hybridization between the plasmon and phonon modes. In particular, the dipole mode (1 and 2 in Figure 2) exhibits a strong hybridization and splits into two distinct peaks. This peak splitting displays the characteristic behavior of an avoided crossing mechanism[20,60] between the phonon and plasmon mode, as also observed experimentally for graphene nanoribbons[24] and graphene nanodisks.[25] Although the spectral width remains almost constant as the size changes, the spectral weight is transferred between the two hybridized dipole peaks, as revealed by comparing the spectra for different sizes in Figure 3b.

The existence of peak splitting signals a strong coupling that exceeds the intrinsic plasmon line width. For example, in the dipole peak near 0.5 eV for 8.1 nm structures in Figure 3a, we notice that a strong coupling regime is reached in which the plasmon-phonon hybridization leads to two dipole peaks below 0.5 eV for 8.1 nm structures in Figure 3b, as opposed to the single peak in the absence of phonons in Figure 3a. These

DOI: 10.1021/acsphotonics.7b00928
ACS Photonics 2017, 4, 2908−2915

features are represented in Figure 4, where we observe similar effects consistently over a large range of triangle sizes.

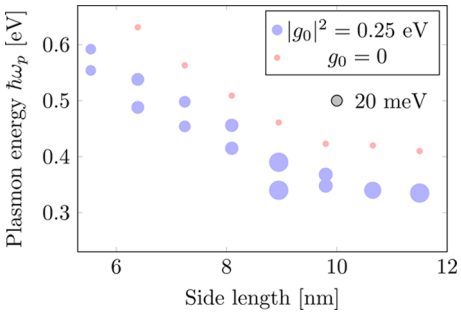

Figure 4. Spectral position of the dipole plasmon peak as a function of the side length of the armchair graphene nanotriangle. The radius of the marks indicates the full-width-half-maximum of the plasmon peak for a phonon density broadening Δ = 5 meV, while for simplicity the g_0 = 0 results exclude such broadening.

Evidently, this strong coupling leading to peak splitting is more effective for small nanotriangles, thereby making phonon interactions especially interesting in the regime of molecular 2D plasmons. In the limit of large structures the plasmon-phonon hybridization becomes less pronounced (results not shown), and we therefore return to the weak coupling regime, in which the phonon interaction broadens and redshifts the plasmon peak.

Plasmon broadening is indicated on Figure 4 through the size of the data points (i.e., the radius indicates the full-width-half-maximum line width of the resonance). For most cases the line width of individual peaks are below ~30 meV, corresponding to plasmon lifetimes of ~20 fs. This is a few times larger than the lifetimes of localized surface plasmons in noble metal nanostructures,[61] but still shorter than the expected lifetimes for plasmons in high-quality extended graphene samples.[17]

As a final illustration of plasmon-phonon coupling, we vary both the electron−phonon coupling strength and the broadening of the phonon density of states, as shown in Figure 5. The peak splitting increases with phonon coupling (Figure 5a), while we require a narrow phonon mode to obtain a well-

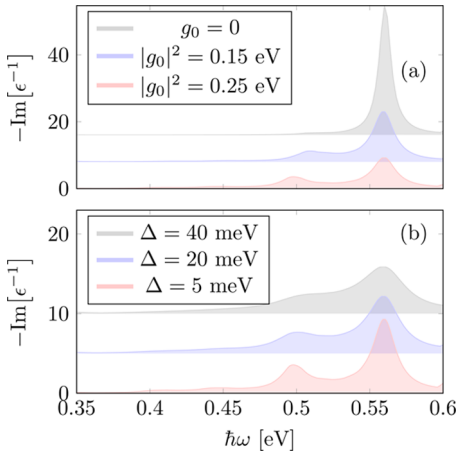

Figure 5. (a) Dipole peak for different values of the electron−phonon coupling in the armchair nanotriangle with side length of 7.2 nm (η = 10 meV). (b) Same dipole peak as in (a) for $|g_0|^2$ = 0.25 eV, but for different values of the broadening, Δ, of the phonon density of states.

defined hybridization and therefore distinguishable hybridization peaks. We insist once more that these calculations also apply for extrinsic phonons of a substrate, incorporated exactly through the same formalism, with appropriately chosen coupling strength and phonon frequency.

DISCUSSION

In this work, we have included a self-energy $\Sigma(\mathcal{E})$ in the single-electron Green function which accounts for the interactions between electrons and other degrees of freedom,[48] and in particular, phonons are considered in the presented examples. Phonons can be hosted by substrates, while they may also be intrinsic to the 2D material. We have limited our study to a spatially constant self-energy, while the formalism can straightforwardly account for spatially dependent couplings to phonons, such as that taking place at atomic edge sites of finite lattices of 2D materials. As an intriguing example of coupling to intrinsic phonons in 2D plasmonics, the understanding of plasmon−phonon coupling in bilayer graphene[62,63] could benefit from application of our method. Naturally, the self-energy could also account for the lifetime broadening of electron states in open quantum systems,[49] where electrons and, consequently, plasmons are quasi-localized to regions of finite extension within an otherwise effectively bulk sheet of graphene. The list of potential geometries can include narrow constrictions (quantum point contacts) in an otherwise infinite ribbon or sheet of graphene,[64] as well as finite graphene antidot arrays[65−67] in extended graphene. We also include on this list nonplanar regions in an otherwise planar sheet of graphene with a local finite surface curvature acting as a trapping potential for electrons and plasmons.[68−73] Localization could likewise be due to local strain and pseudomagnetic fields.[74] The explicit energy dependence of $\Sigma(\mathcal{E})$ is common to these problems and reflects the energy dependence of the density-of-states in the surrounding medium. Because of this, the lifetime broadening would not be captured accurately by a phenomenological constant damping rate.

CONCLUSION

We have introduced a computationally highly efficient approach to describe the optical response of plasmonic nanostructures that facilitates the inclusion of many-body interactions. This formalism neglects vertex corrections, which is a valid approximation for metallic nanostructures or 2D Dirac-Fermion systems, such as graphene. Here, we have illustrated the power of our method for armchair graphene nanotriangles of various sizes, paying special attention to the evaluation of eigenvalue loss-spectra for plasmons dressed by optical phonons. The interactions with phonons are represented by self-energies that enter the electron Green function, and we emphasize that the energy dependence of the self-energies leads to qualitative changes in the spectra that cannot simply be accounted for by a more phenomenological broadening, such as inclusion of a complex-valued substrate dielectric function. As an example, the hybridization between plasmons and phonons manifests in dramatic peak splitting. While we have focused on interactions with phonons, we may without further complications apply our self-energy formalism to account for other types of nanostructures and interactions relevant to quantum plasmonics,[34,35,75,76] including also dephasing phenomena and lifetime broadening in open quantum systems, where the electron gas remains only quasi confined.

DOI: 10.1021/acsphotonics.7b00928
ACS Photonics 2017, 4, 2908−2915

■ ASSOCIATED CONTENT

Supporting Information

The Supporting Information is available free of charge on the ACS Publications website at DOI: 10.1021/acsphotonics.7b00928.

We provide further details on the recursive Green function approach, the χ^0 calculation, and our use of the Kramers−Kronig relation (PDF).

■ AUTHOR INFORMATION

Corresponding Author

*E-mail: asger@mailaps.org.

ORCID

Kristian S. Thygesen: 0000-0001-5197-214X

N. Asger Mortensen: 0000-0001-7936-6264

Notes

The authors declare no competing financial interest.

■ ACKNOWLEDGMENTS

We thank Christian Wolff for stimulating discussions on the numerics and useful comments on an initial version of this manuscript. The Center for Nanostructured Graphene is supported by the Danish National Research Foundation (DNRF103). This work is partially supported by the European Commission (Graphene Flagship CNECT- ICT-604391 and FP7-ICT-2013-613024-GRASP) and the Spanish MINECO (MAT2014-59096-P, Fundació Privada Cellex, and SEV2015-0522). J.R.M.S. acknowledges financial support through AGAUR FI B 00492-2015. M.S. and N.A.M. acknowledge support from the Danish Council for Independent Research (DFF-5051-00011 & DFF 1323-00087). N.A.M. is a VILLUM Investigator supported by VILLUM Fonden (Grant No. 16498).

■ REFERENCES

(1) Basov, D. N.; Fogler, M. M.; García de Abajo, F. J. Polaritons in van der Waals materials. *Science* **2016**, *354*, 195.

(2) Low, T.; Chaves, A.; Caldwell, J. D.; Kumar, A.; Fang, N. X.; Avouris, P.; Heinz, T. F.; Guinea, F.; Martín-Moreno, L.; Koppens, F. Polaritons in layered two-dimensional materials. *Nat. Mater.* **2016**, *16*, 182−194.

(3) Fei, Z.; Rodin, A. S.; Andreev, G. O.; Bao, W.; McLeod, A. S.; Wagner, M.; Zhang, L. M.; Zhao, Z.; Thiemens, M.; Dominguez, G.; Fogler, M. M.; Castro-Neto, A. H.; Lau, C. N.; Keilmann, F.; Basov, D. N. Gate-tuning of graphene plasmons revealed by infrared nano-imaging. *Nature* **2012**, *487*, 82−85.

(4) Chen, J.; Badioli, M.; Alonso-González, P.; Thongrattanasiri, S.; Huth, F.; Osmond, J.; Spasenović, M.; Centeno, A.; Pesquera, A.; Godignon, P.; Zurutuza Elorza, A.; Camara, N.; García de Abajo, F. J.; Hillenbrand, R.; Koppens, F. H. L. Optical nano-imaging of gate-tunable graphene plasmons. *Nature* **2012**, *487*, 77−81.

(5) Dai, S.; et al. Tunable Phonon Polaritons in Atomically Thin van der Waals Crystals of Boron Nitride. *Science* **2014**, *343*, 1125−1129.

(6) Caldwell, J. D.; Kretinin, A. V.; Chen, Y.; Giannini, V.; Fogler, M. M.; Francescato, Y.; Ellis, C. T.; Tischler, J. G.; Woods, C. R.; Giles, A. J.; Hong, M.; Watanabe, K.; Taniguchi, T.; Maier, S. A.; Novoselov, K. S. Sub-diffractional volume-confined polaritons in the natural hyperbolic material hexagonal boron nitride. *Nat. Commun.* **2014**, *5*, 5221.

(7) Caldwell, J. D.; Lindsay, L.; Giannini, V.; Vurgaftman, I.; Reinecke, T. L.; Maier, S. A.; Glembocki, O. J. Low-loss, infrared and terahertz nanophotonics using surface phonon polaritons. *Nanophotonics* **2015**, *4*, 44−68.

(8) García de Abajo, F. J. Graphene Plasmonics: Challenges and Opportunities. *ACS Photonics* **2014**, *1*, 135−152.

(9) Xiao, S.; Zhu, X.; Li, B.-H.; Mortensen, N. A. Graphene-plasmon polaritons: From fundamental properties to potential applications. *Front. Phys.* **2016**, *11*, 117801.

(10) Gonçalves, P. A. D.; Peres, N. M. R. *An Introduction to Graphene Plasmonics*; World Scientific: Singapore, 2016; DOI: 10.1142/9948.

(11) Huang, S.; Song, C.; Zhang, G.; Yan, H. Graphene plasmonics: physics and potential applications. *Nanophotonics* **2017**, *6*, 1191−1204.

(12) Bolotin, K.; Sikes, K.; Jiang, Z.; Klima, M.; Fudenberg, G.; Hone, J.; Kim, P.; Stormer, H. Ultrahigh electron mobility in suspended graphene. *Solid State Commun.* **2008**, *146*, 351.

(13) Fratini, S.; Guinea, F. Substrate-limited electron dynamics in graphene. *Phys. Rev. B: Condens. Matter Mater. Phys.* **2008**, *77*, 195415.

(14) Politano, A. Spectroscopic Investigations of Phonons in Epitaxial Graphene. *Crit. Rev. Solid State Mater. Sci.* **2017**, *42*, 99−128.

(15) Hess, K.; Vogl, P. Remote polar phonon-scattering in silicon inversion layers. *Solid State Commun.* **1979**, *30*, 807−809.

(16) Dean, C. R.; Young, A. F.; Meric, I.; Lee, C.; Wang, L.; Sorgenfrei, S.; Watanabe, K.; Taniguchi, T.; Kim, P.; Shepard, K. L.; Hone, J. Boron nitride substrates for high-quality graphene electronics. *Nat. Nanotechnol.* **2010**, *5*, 722−726.

(17) Woessner, A.; Lundeberg, M. B.; Gao, Y.; Principi, A.; Alonso-Gonzaolez, P.; Carrega, M.; Watanabe, K.; Taniguchi, T.; Vignale, G.; Polini, M.; Hone, J.; Hillenbrand, R.; Koppens, F. H. L. Highly confined low-loss plasmons in graphene-boron nitride heterostructures. *Nat. Mater.* **2014**, *14*, 421−425.

(18) Principi, A.; Carrega, M.; Lundeberg, M. B.; Woessner, A.; Koppens, F. H. L.; Vignale, G.; Polini, M. Plasmon losses due to electron-phonon scattering: The case of graphene encapsulated in hexagonal boron nitride. *Phys. Rev. B: Condens. Matter Mater. Phys.* **2014**, *90*, 165408.

(19) Hwang, E. H.; Sensarma, R.; Das Sarma, S. Plasmon-phonon coupling in graphene. *Phys. Rev. B: Condens. Matter Mater. Phys.* **2010**, *82*, 195406.

(20) Jablan, M.; Soljačić, M.; Buljan, H. Unconventional plasmon-phonon coupling in graphene. *Phys. Rev. B: Condens. Matter Mater. Phys.* **2011**, *83*, 161409.

(21) Liu, Y.; Willis, R. F. Plasmon-phonon strongly coupled mode in epitaxial graphene. *Phys. Rev. B: Condens. Matter Mater. Phys.* **2010**, *81*, 081406.

(22) Koch, R. J.; Seyller, T.; Schaefer, J. A. Strong phonon-plasmon coupled modes in the graphene/silicon carbide heterosystem. *Phys. Rev. B: Condens. Matter Mater. Phys.* **2010**, *82*, 201413.

(23) Fei, Z.; et al. Infrared nanoscopy of Dirac plasmons at the graphene-SiO_2 interface. *Nano Lett.* **2011**, *11*, 4701−4705.

(24) Yan, H.; Low, T.; Zhu, W.; Wu, Y.; Freitag, M.; Li, X.; Guinea, F.; Avouris, P.; Xia, F. Damping pathways of mid-infrared plasmons in graphene nanostructures. *Nat. Photonics* **2013**, *7*, 394−399.

(25) Zhu, X.; Wang, W.; Yan, W.; Larsen, M. B.; Bøggild, P.; Pedersen, T. G.; Xiao, S.; Zi, J.; Mortensen, N. A. Plasmon-Phonon Coupling in Large-Area Graphene Dot and Antidot Arrays Fabricated by Nanosphere Lithography. *Nano Lett.* **2014**, *14*, 2907−2913.

(26) Li, Y.; Yan, H.; Farmer, D. B.; Meng, X.; Zhu, W.; Osgood, R. M.; Heinz, T. F.; Avouris, P. Graphene Plasmon Enhanced Vibrational Sensing of Surface-Adsorbed Layers. *Nano Lett.* **2014**, *14*, 1573−1577.

(27) Brar, V. W.; Jang, M. S.; Sherrott, M.; Kim, S.; Lopez, J. J.; Kim, L. B.; Choi, M.; Atwater, H. Hybrid Surface-Phonon-Plasmon Polariton Modes in Graphene/Monolayer h-BN Heterostructures. *Nano Lett.* **2014**, *14*, 3876−3880.

(28) Barcelos, I. D.; Cadore, A. R.; Campos, L. C.; Malachias, A.; Watanabe, K.; Taniguchi, T.; Maia, F. C. B.; Freitas, R.; Deneke, C. Graphene/h-BN plasmon-phonon coupling and plasmon delocalization observed by infrared nano-spectroscopy. *Nanoscale* **2015**, *7*, 11620−11625.

(29) Gunst, T.; Kaasbjerg, K.; Brandbyge, M. Flexural-Phonon Scattering Induced by Electrostatic Gating in Graphene. *Phys. Rev. Lett.* **2017**, *118*, 046601.

DOI: 10.1021/acsphotonics.7b00928
ACS Photonics 2017, 4, 2908−2915

(30) Thongrattanasiri, S.; Manjavacas, A.; García de Abajo, F. J. Quantum Finite-Size Effects in Graphene Plasmons. *ACS Nano* **2012**, *6*, 1766−1775.
(31) Christensen, T.; Wang, W.; Jauho, A.-P.; Wubs, M.; Mortensen, N. A. Classical and quantum plasmonics in graphene nanodisks: Role of edge states. *Phys. Rev. B: Condens. Matter Mater. Phys.* **2014**, *90*, 241414.
(32) Wang, W.; Christensen, T.; Jauho, A.-P.; Thygesen, K. S.; Wubs, M.; Mortensen, N. A. Plasmonic eigenmodes in individual and bow-tie graphene nanotriangles. *Sci. Rep.* **2015**, *5*, 9535.
(33) Stauber, T. Plasmonics in Dirac systems: from graphene to topological insulators. *J. Phys.: Condens. Matter* **2014**, *26*, 123201.
(34) Tame, M. S.; McEnery, K. R.; Özdemir, S. K.; Lee, J.; Maier, S. A.; Kim, M. S. Quantum plasmonics. *Nat. Phys.* **2013**, *9*, 329−340.
(35) Bozhevolnyi, S. I.; Mortensen, N. A. Plasmonics for emerging quantum technologies. *Nanophotonics* **2017**, *6*, 1185−1188.
(36) Bozhevolnyi, S. I., Martín-Moreno, L., García-Vidal, F. J., Eds. *Quantum Plasmonics*; Springer Series in Solid-State Sciences; Springer International Publishing: Cham, Switzerland, 2017; Vol. *185*; DOI: 10.1007/978-3-319-45820-5.
(37) Raza, S.; Bozhevolnyi, S. I.; Wubs, M.; Mortensen, N. A. Nonlocal optical response in metallic nanostructures. *J. Phys.: Condens. Matter* **2015**, *27*, 183204.
(38) Varas, A.; García-González, P.; Feist, J.; García-Vidal, F. J.; Rubio, A. Quantum plasmonics: from jellium models to ab initio calculations. *Nanophotonics* **2016**, *5*, 409−426.
(39) Thygesen, K. S. Calculating excitons, plasmons, and quasiparticles in 2D materials and van der Waals heterostructures. *2D Mater.* **2017**, *4*, 022004.
(40) Huber, M. A.; Mooshammer, F.; Plankl, M.; Viti, L.; Sandner, F.; Kastner, L. Z.; Frank, T.; Fabian, J.; Vitiello, M. S.; Cocker, T. L.; Huber, R. Femtosecond Photo-Switching of Interface Polaritons in Black Phosphorus Heterostructures. *Nat. Nanotechnol.* **2016**, *12*, 207−212.
(41) Manjavacas, A.; García de Abajo, F. J. Tunable plasmons in atomically thin gold nanodisks. *Nat. Commun.* **2014**, *5*, 3548.
(42) Bruus, H.; Flensberg, K. *Many-Body Quantum Theory in Condensed Matter Physics: An Introduction*; Oxford University Press: Oxford, 2004.
(43) Andersen, K.; Jacobsen, K. W.; Thygesen, K. S. Spatially resolved quantum plasmon modes in metallic nano-films from first-principles. *Phys. Rev. B: Condens. Matter Mater. Phys.* **2012**, *86*, 245129.
(44) Andersen, K.; Thygesen, K. S. Plasmons in metallic monolayer and bilayer transition metal dichalcogenides. *Phys. Rev. B: Condens. Matter Mater. Phys.* **2013**, *88*, 155128.
(45) Andersen, K.; Jensen, K. L.; Mortensen, N. A.; Thygesen, K. S. Visualizing hybridized quantum plasmons in coupled nanowires: From classical to tunneling regime. *Phys. Rev. B: Condens. Matter Mater. Phys.* **2013**, *87*, 235433.
(46) García de Abajo, F. J. Optical excitations in electron microscopy. *Rev. Mod. Phys.* **2010**, *82*, 209−275.
(47) Prange, M. P.; Rehr, J. J.; Rivas, G.; Kas, J. J.; Lawson, J. W. Real space calculation of optical constants from optical to x-ray frequencies. *Phys. Rev. B: Condens. Matter Mater. Phys.* **2009**, *80*, 155110.
(48) Haug, H.; Jauho, A.-P. *Quantum Kinetics in Transport and Optics of Semiconductors*; Springer, 2008; DOI: 10.1007/978-3-540-73564-9.
(49) Datta, S. *Electronic Transport in Mesoscopic Systems*; Cambridge University Press: Cambridge, 1995; DOI: 10.1017/CBO9780511805776.
(50) Roy, B.; Sau, J. D.; Das Sarma, S. Migdal's theorem and electron-phonon vertex corrections in Dirac materials. *Phys. Rev. B: Condens. Matter Mater. Phys.* **2014**, *89*, 165119.
(51) Settnes, M.; Power, S. R.; Lin, J.; Petersen, D. H.; Jauho, A.-P. Patched Green's function techniques for two-dimensional systems: Electronic behavior of bubbles and perforations in graphene. *Phys. Rev. B: Condens. Matter Mater. Phys.* **2015**, *91*, 125408.
(52) Lewenkopf, C. H.; Mucciolo, E. R. The recursive Green's function method for graphene. *J. Comput. Electron.* **2013**, *12*, 203−231.
(53) Nakada, K.; Fujita, M.; Dresselhaus, G.; Dresselhaus, M. S. Edge state in graphene ribbons: Nanometer size effect and edge shape dependence. *Phys. Rev. B: Condens. Matter Mater. Phys.* **1996**, *54*, 17954−17961.
(54) Potasz, P.; Güçlü, A. D.; Hawrylak, P. Zero-energy states in triangular and trapezoidal graphene structures. *Phys. Rev. B: Condens. Matter Mater. Phys.* **2010**, *81*, 033403.
(55) Manjavacas, A.; Thongrattanasiri, S.; García de Abajo, F. J. Plasmons driven by single electrons in graphene nanoislands. *Nanophotonics* **2013**, *2*, 139−151.
(56) Awada, C.; Popescu, T.; Douillard, L.; Charra, F.; Perron, A.; Yockell-Leliévre, H.; Baudrion, A.-L.; Adam, P.-M.; Bachelot, R. Selective Excitation of Plasmon Resonances of Single Au Triangles by Polarization-Dependent Light Excitation. *J. Phys. Chem. C* **2012**, *116*, 14591−14598.
(57) Park, C.-H.; Giustino, F.; Cohen, M. L.; Louie, S. G. Velocity Renormalization and Carrier Lifetime in Graphene from the Electron-Phonon Interaction. *Phys. Rev. Lett.* **2007**, *99*, 086804.
(58) Carbotte, J. P.; Nicol, E. J.; Sharapov, S. G. Effect of electron-phonon interaction on spectroscopies in graphene. *Phys. Rev. B: Condens. Matter Mater. Phys.* **2010**, *81*, 045419.
(59) Jablan, M.; Buljan, H.; Soljačić, M. Plasmonics in graphene at infrared frequencies. *Phys. Rev. B: Condens. Matter Mater. Phys.* **2009**, *80*, 245435.
(60) Hwang, E. H.; Sensarma, R.; Das Sarma, S. Plasmon-phonon coupling in graphene. *Phys. Rev. B: Condens. Matter Mater. Phys.* **2010**, *82*, 195406.
(61) Maier, S. A. *Plasmonics: Fundamentals and Applications*; Springer: New York, NY, 2007; DOI: 10.1007/0-387-37825-1.
(62) Low, T.; Guinea, F.; Yan, H.; Xia, F.; Avouris, P. Novel Midinfrared Plasmonic Properties of Bilayer Graphene. *Phys. Rev. Lett.* **2014**, *112*, 116801.
(63) Yan, H.; Low, T.; Guinea, F.; Xia, F.; Avouris, P. Tunable Phonon-Induced Transparency in Bilayer Graphene Nanoribbons. *Nano Lett.* **2014**, *14*, 4581−4586.
(64) Tombros, N.; Veligura, A.; Junesch, J.; Guimarães, M. H. D.; Vera-Marun, I. J.; Jonkman, H. T.; van Wees, B. J. Quantized conductance of a suspended graphene nanoconstriction. *Nat. Phys.* **2011**, *7*, 697−700.
(65) Pedersen, T. G.; Flindt, C.; Pedersen, J.; Mortensen, N. A.; Jauho, A.-P.; Pedersen, K. Graphene Antidot Lattices: Designed Defects and Spin Qubits. *Phys. Rev. Lett.* **2008**, *100*, 136804.
(66) Jin, D.; Christensen, T.; Soljačić, M.; Fang, N. X.; Lu, L.; Zhang, X. Infrared Topological Plasmons in Graphene. *Phys. Rev. Lett.* **2017**, *118*, 245301.
(67) Pan, D.; Yu, R.; Xu, H.; García de Abajo, F. J. Topologically protected Dirac plasmons in graphene. *arXiv:1702.00036* **2017**, na.
(68) Wang, W.; Li, B.-H.; Stassen, E.; Mortensen, N. A.; Christensen, J. Localized surface plasmons in vibrating graphene nanodisks. *Nanoscale* **2016**, *8*, 3809−3815.
(69) Smirnova, D.; Mousavi, S. H.; Wang, Z.; Kivshar, Y. S.; Khanikaev, A. B. Trapping and Guiding Surface Plasmons in Curved Graphene Landscapes. *ACS Photonics* **2016**, *3*, 875−880.
(70) Gonçalves, P. A. D.; Dias, E. J. C.; Xiao, S.; Vasilevskiy, M. I.; Mortensen, N. A.; Peres, N. M. R. Graphene Plasmons in Triangular Wedges and Grooves. *ACS Photonics* **2016**, *3*, 2176−2183.
(71) Gonçalves, P. A. D.; Bozhevolnyi, S. I.; Mortensen, N. A.; Peres, N. M. R. Universal description of channel plasmons in two-dimensional materials. *Optica* **2017**, *4*, 595−600.
(72) Fei, Z.; Foley, J. J.; Gannett, W.; Liu, M. K.; Dai, S.; Ni, G. X.; Zettl, A.; Fogler, M. M.; Wiederrecht, G. P.; Gray, S. K.; Basov, D. N. Ultraconfined Plasmonic Hotspots Inside Graphene Nanobubbles. *Nano Lett.* **2016**, *16*, 7842−7848.
(73) Slipchenko, T.; Nesterov, M. L.; Hillenbrand, R.; Nikitin, A. Y.; Martín-Moreno, L. Graphene Plasmon Reflection by Corrugations. *ACS Photonics* **2017**, ASAP.
(74) Settnes, M.; Power, S. R.; Brandbyge, M.; Jauho, A.-P. Graphene Nanobubbles as Valley Filters and Beam Splitters. *Phys. Rev. Lett.* **2016**, *117*, 276801.

DOI: 10.1021/acsphotonics.7b00928
ACS Photonics 2017, 4, 2908−2915

(75) Fitzgerald, J. M.; Narang, P.; Craster, R. V.; Maier, S. A.; Giannini, V. Quantum Plasmonics. *Proc. IEEE* **2016**, *104*, 2307−2322.
(76) Zhu, W.; Esteban, R.; Borisov, A. G.; Baumberg, J. J.; Nordlander, P.; Lezec, H. J.; Aizpurua, J.; Crozier, K. B. Quantum mechanical effects in plasmonic structures with subnanometre gaps. *Nat. Commun.* **2016**, *7*, 11495.

DOI: 10.1021/acsphotonics.7b00928
ACS Photonics 2017, 4, 2908−2915

Strong plasmon-phonon splitting and hybridization in 2D materials revealed through a self-energy approach — Supporting Information

Mikkel Settnes, J. R. M. Saavedra, Kristian S. Thygesen, Antti-Pekka Jauho, F. Javier García de Abajo, and N. Asger Mortensen*

E-mail: asger@mailaps.org

The recursive Green function approach

For small, closed systems one may obtain the electron Green function [Eq. (9) in the main text] through a direct matrix inversion of the Hamiltonian. Here, we provide a brief account on the numerical implementation of our method to calculate the electron Green function for larger systems where a more efficient approach is needed.

The numerical procedure to determine the electron Green function follows Refs. 1,2 and it is described in detail in Ref. 3. The approach offers a numerically efficient technique to evaluate the Green function for extended two-dimensional systems without relying on periodic boundary conditions. Different regions of interest, or *patches*, are connected using self-energy terms which encode the information of the extended parts of the system. The calculation scheme uses a combination of analytic expressions for the Green's function of infinite pristine systems and an adaptive recursive Green function technique for the patches. The method allows for an efficient calculation of both local electronic and transport proper-

ties, as well as the inclusion of multiple probes in arbitrary geometries embedded in extended samples.

1 χ^0 calculation

The imaginary part of $\chi^0(\vec{r},\vec{r}',\omega)$ can be determined from Eq. (8) in the main text. We calculate the Green function (and by extension the spectral function) for all energies from $\mathscr{E}_F - \hbar\omega_{max}$ to $\mathscr{E}_F + \hbar\omega_{max}$ with a finite spacing of $\delta\mathscr{E}$, where $\hbar\omega_{max}$ is a maximum energy cut-off ensuring that the integration [Eq. (8)] is accurate. The maximum energy cut-off and the energy spacing are convergence parameters. For larger structures, we use an energy cut-off of 8 eV and an energy spacing of 1 meV.

The Green functions can be stored and re-used to calculate $\chi^0(\vec{r},\vec{r}',\omega)$ for all energies using convolution-type algorithms available in standard numerical packages. When $\chi^0(\vec{r},\vec{r}',\omega)$ has been determined, we use the Kramers–Kronig relation to determine the real part. The details are described in the next section.

2 Kramers–Kronig relation

We determine the real part of $\chi^0_R(\omega)$ from the imaginary part $\chi^0_I(\omega)$. Due to causality of the response function, this can be done using the Kramers–Kronig relation

$$\chi^0_R(\omega) = \frac{1}{\pi} P \int_0^\infty dx\, \frac{\chi^0_I(x)}{x-\omega} + \frac{1}{\pi} P \int_0^\infty dx\, \frac{\chi^0_I(x)}{x+\omega}, \tag{1}$$

where P denotes Cauchy's principal part. The Kramers–Kronig integration can be replaced by a weighted sum,[4]

$$\chi^0_R(\omega_i) = \sum_n W_n(\omega_i)\chi^0_I(\omega_n), \tag{2a}$$

where the weight factors are calculated using

$$W_n(\omega_i) = \frac{1}{\pi} P \int_0^\infty dx\, \Phi_n(x) \left(\frac{1}{x - \omega_i} + \frac{1}{x + \omega_i} \right) \tag{2b}$$

with

$$\Phi_n(x) = \begin{cases} \frac{\omega_{n+1} - x}{\omega_{n+1} - \omega_n} & , \quad \omega_n \leq x \leq \omega_{n+1} \\ \frac{x - \omega_{n-1}}{\omega_n - \omega_{n-1}} & , \quad \omega_{n-1} \leq x \leq \omega_n \\ 0 & , \quad \text{otherwise} \end{cases} \tag{2c}$$

To determine the weight factors, we consider the integral Eq. (2b) and insert Eq. (2c) to obtain an analytical expression for W_n,

$$W_n(\omega_i) = \frac{1}{\pi(\omega_n - \omega_{n-1})} \Bigg[(\omega_i - \omega_{n-1}) \log \left| \frac{\omega_n - \omega_i}{\omega_{n-1} - \omega_i} \right| - (\omega_i + \omega_{n-1}) \log \left| \frac{\omega_n + \omega_i}{\omega_{n-1} + \omega_i} \right| \\ - (\omega_i - \omega_{n+1}) \log \left| \frac{\omega_{n+1} - \omega_i}{\omega_n - \omega_i} \right| + (\omega_i + \omega_{n+1}) \log \left| \frac{\omega_{n+1} + \omega_i}{\omega_n + \omega_i} \right| \Bigg]. \tag{3}$$

This procedure allows us to replace the integral with a summation in order to obtain χ_R^0 on a grid containing the mid-points of the original grid in which χ_I^0 was determined. Linear interpolation can be used efficiently to produce χ_I^0 and χ_R^0 on the same grid.

References

(1) Settnes, M.; Power, S. R.; Lin, J.; Petersen, D. H.; Jauho, A.-P. Patched Green's function techniques for two-dimensional systems: Electronic behavior of bubbles and perforations in graphene. *Phys. Rev. B* **2015**, *91*, 125408.

(2) Lewenkopf, C. H.; Mucciolo, E. R. The recursive Green's function method for graphene. *J. Comput. Electron.* **2013**, *12*, 203–231.

(3) Settnes, M. Theory of dual probes on graphene nanostructures. Ph.D. thesis,

Technical University of Denmark, 2015; http://emagstudio.win.dtu.dk/E-books/DTUNanotech/PhDthesisbyMikkelSettnes.

(4) Shishkin, M.; Kresse, G. Implementation and performance of the frequency-dependent *GW* method within the PAW framework. *Phys. Rev. B* **2006**, *74*, 035101.